

**Secondary organic
aerosol from
NO₃+limonene**

J. L. Fry et al.

SOA from limonene: role of NO₃ in its generation and degradation

J. L. Fry^{1,*}, A. Kiendler-Scharr², A. W. Rollins¹, T. Brauers², S. S. Brown³,
H.-P. Dorn², W. P. Dubé³, H. Fuchs^{3,**}, A. Mensah², F. Rohrer², R. Tillmann²,
A. Wahner², P. J. Wooldridge¹, and R. C. Cohen¹

¹Department of Chemistry, University of California, Berkeley, CA, USA

²ICG-2: Troposphäre, Forschungszentrum Jülich, 52425 Jülich, Germany

³Chemical Sciences Division, NOAA Earth System Research Laboratory, Boulder, CO, USA

*now at: Chemistry Department, Reed College, Portland, OR, USA

**now at: ICG-2: Troposphäre, Forschungszentrum Jülich, 52425 Jülich, Germany

Received: 6 December 2010 – Accepted: 7 December 2010 – Published: 22 December 2010

Correspondence to: R. C. Cohen (rccohen@berkeley.edu)

Published by Copernicus Publications on behalf of the European Geosciences Union.

Title Page

Abstract

Introduction

Conclusions

References

Tables

Figures

◀

▶

◀

▶

Back

Close

Full Screen / Esc

Printer-friendly Version

Interactive Discussion



Abstract

The formation of organic nitrates and secondary organic aerosol (SOA) were monitored during the NO_3 +limonene reaction in the atmosphere simulation chamber SAPHIR at Research Center Jülich. The 24-h run began in a purged, dry, particle-free chamber and comprised two injections of limonene and oxidants, such that the first experiment measured SOA yield in the absence of seed aerosol, and the second experiment yields in the presence of $10 \mu\text{g m}^{-3}$ seed organic aerosol. After each injection, two separate increases in aerosol mass were observed, corresponding to sequential oxidation of the two limonene double bonds. Analysis of the measured NO_3 , limonene, product nitrate concentrations, and aerosol properties provides mechanistic insight and constrains rate constants, branching ratios and vapor pressures of the products. The organic nitrate yield from NO_3 +limonene is $\approx 30\%$. The SOA mass yield was observed to be 25–40%. The first injection is reproduced by a kinetic model. PMF analysis of the aerosol composition suggests that much of the aerosol mass results from combined oxidation by both O_3 and NO_3 , e.g., oxidation of NO_3 +limonene products by O_3 . Further, later aerosol nitrate mass seems to derive from heterogeneous uptake of NO_3 onto unreacted aerosol alkene.

1 Introduction

Biogenic volatile organic compounds (BVOCs) make up a large fraction of gas-phase organic compounds emitted to the atmosphere: on a global scale, vegetation emissions of VOCs are an order of magnitude greater than those from petrochemicals (Guenther et al., 1995). Furthermore, in the atmosphere, many of these compounds are rapidly oxidized and likely to form condensable products (Griffin et al., 1999). Among these compounds, monoterpenes are known to be important sources of secondary organic aerosol (SOA) (Goldstein and Galbally, 2007; Eerdekens et al., 2009; Tunved et al., 2006; Slowik et al., 2010; Hallquist et al., 1999).

Secondary organic aerosol from NO_3 +limonene

J. L. Fry et al.

Title Page

Abstract

Introduction

Conclusions

References

Tables

Figures

◀

▶

◀

▶

Back

Close

Full Screen / Esc

Printer-friendly Version

Interactive Discussion



**Secondary organic
aerosol from
NO₃+limonene**

J. L. Fry et al.

Title Page

Abstract

Introduction

Conclusions

References

Tables

Figures

◀

▶

◀

▶

Back

Close

Full Screen / Esc

Printer-friendly Version

Interactive Discussion



If NO₃-initiated aerosol formation from biogenic VOCs is a significant contribution to organic aerosol loading in the atmosphere, this would provide a potential resolution to a paradox noted in the SOA literature: ¹⁴C measurements show the carbon in organic aerosol to be primarily modern, which is characteristic of natural emissions, from urban (≈50%) to remote areas (80–100%) (Schichtel et al., 2008). However, aerosol loading in both urban and rural areas is observed to be correlated to aging in anthropogenic emissions plumes (de Gouw et al., 2005; Quinn et al., 2006; Weber et al., 2007). NO₃ produced BVOC SOA resolves the paradox by requiring both an anthropogenic oxidant “trigger” and biogenic VOC to form aerosol. This mechanism of SOA formation is expected to be most significant in forested areas downwind of urban centers or power plants, where NO_x is high and biogenic VOCs are abundant (Pye et al., 2010). Because the nitrate radical is photolabile, this mechanism is also expected to be most important at night or within a shaded forest canopy.

Limonene is of interest as a representative BVOC both due to its high emission rate among monoterpenes (Sakulyanontvittaya et al., 2008) and its possession of two double bonds. These two reactive sites for oxidation give limonene a rapid and direct route to the types of low-vapor pressure oxidized products that are likely to form secondary organic aerosol. As a consequence, limonene may contribute disproportionately to total SOA relative to other terpenoids (Lane et al., 2008; Maksymiuk et al., 2009). Further, limonene’s frequent use in household cleaning products and air fresheners makes it a common source of indoor air pollution when its oxidation results in aerosol formation (Wainman et al., 2000). Aerosol formation from the reaction of NO₃ with limonene has been the subject of a previous chamber study (Spittler et al., 2006); in excess limonene and no O₃, organic nitrates were formed in high yield (67%), accompanied by immediate SOA formation.

Here we report chamber measurements and kinetic modeling of gas- and aerosol-phase chemistry during SOA formation initiated by the NO₃+limonene reaction under excess oxidants.

2 Experimental

2.1 Atmosphere simulation chamber SAPHIR

The experiment described below was conducted on the 16 and 17 of June 2007 in the atmospheric simulation chamber SAPHIR at Research Center Jülich as part of the intercomparison campaign of NO₃ (Dorn et al., 2010), N₂O₅ (Apodaca et al., 2010), and NO₂ (Fuchs et al., 2009) measurements. The SAPHIR chamber is a large (270 m³) cylindrical chamber with double walls made from FEP film. It is equipped with an automated shuttering system to enable simulation of day or night conditions. The chamber and its operation during simulation experiments has been described in detail (e.g., Rohrer et al., 2005; Bohn and Zilken, 2005; Wegener et al., 2007). The chamber was used for large instrument intercomparison campaigns (e.g., Apel et al., 2008; Schlosser et al., 2009) and it was shown to serve as an excellent platform for multi-instrument experiments. Only a brief description of the chamber instruments and chamber operation is presented in the following.

The chamber has standard instrumentation for measurement of NO (chemiluminescence), NO_x, temperature, pressure, humidity, dilution flow, and O₃ (UV-absorption). However, during this experiment ozone concentrations were measured by chemiluminescence in a modified ECO Physics CLD AL 700 (Ridley et al., 1992). A GC-FID system (Perkin-Elmer) was used to verify the cleanness after purging and to follow the ethane concentration as an inert tracer of dilution. The limonene concentration was measured by Proton Transfer Reaction Mass Spectrometry (PTR-MS, IONICON, Austria; Lindinger et al., 1998).

Before the experiment, the chamber was purged overnight to ppt levels of nitrogen oxides, ozone, and hydrocarbons using a large flow 300 m³/h of clean synthetic air (N₂, O₂, purity >99.9999%). During the experiment, the pressure was maintained at 30–50 hPa above ambient to prevent contamination. The slight overpressure was held by a smaller replenishment flow of the same synthetic air as used for flushing. During the entire experiment a fan provided fast mixing of constituents within the chamber. Due

Secondary organic aerosol from NO₃+limonene

J. L. Fry et al.

Title Page

Abstract

Introduction

Conclusions

References

Tables

Figures

◀

▶

◀

▶

Back

Close

Full Screen / Esc

Printer-friendly Version

Interactive Discussion



to the replenishment flow of 10–15 m³/h all gases were diluted by a rate of ≈4–5.5%/h. The shutter system was closed throughout the experiment, keeping the chamber in darkness.

The trace gases (NO₂, ethane, and limonene) were added to the replenishment flow. Ozone (≈5%) was produced by silent discharge in pure oxygen and injected into the chamber. Before the reaction started, 500 ppm of CO was added to the chamber in order to scavenge any OH formed.

2.2 NO₃, N₂O₅, and NO_y measurements

During the intercomparison campaign several instruments measuring NO₃ and N₂O₅ concentrations were operated at SAPHIR (Dorn et al., 2010; Apodaca et al., 2010). Here we employ the data set from one of the instruments, the Cavity Ring-Down Spectrometer (CRDS) of the NOAA Earth System Research Lab team (Dube et al., 2006; Fuchs et al., 2008). None of the conclusions of this manuscript depend strongly on the choice of the NO₃+N₂O₅ measurement, as all measurements agreed to within 20%.

NO₂ was measured by laser-induced fluorescence (LIF) and total peroxy nitrates (ΣPNs), total alkyl and multifunctional nitrates (ΣANs), and nitric acid (HNO₃) were determined using thermal dissociation to NO₂ in heated quartz ovens held at different temperatures (“NO₂-TD-LIF”) (Thornton et al., 2000; Day et al., 2002). Details of this instrument are described in Wooldridge et al. (2010).

Briefly, the NO₂-TD-LIF instrument sampled at 3 standard liters per minute (slpm) from ca. 10 cm above the floor of the SAPHIR chamber through a Teflon PFA inlet (40 cm of 3.2 mm inner diameter tubing). A glass capillary orifice was used to reduce pressure, and the sample was split to four channels. In the ambient temperature channel NO₂ is detected. The other channels are held at 180 °C, 350 °C, and 600 °C, where ΣPNs, ΣANs, and HNO₃ dissociate to yield NO₂. The mixing ratio of each class of nitrate is calculated from the difference in total NO₂ measured in adjacent temperature channels. We expect both gaseous and semivolatile aerosol-phase nitrates to dissociate completely, while thermally stable salts such as NaNO₃ will not be detected.

Secondary organic aerosol from NO₃+limonene

J. L. Fry et al.

Title Page

Abstract

Introduction

Conclusions

References

Tables

Figures

◀

▶

◀

▶

Back

Close

Full Screen / Esc

Printer-friendly Version

Interactive Discussion



The NO₂ concentration in the reduced-pressure sample flow ($P \approx 1.5$ Torr, 200 Pa) is detected by LIF. Here, we excite with a 408 nm continuous-wave diode laser at (8 mW, Toptica Photonics DL100) and collect filtered red-shifted fluorescence ($\lambda > 650$ nm) with a photomultiplier tube (PMT, Hamamatsu H7421-50) mounted at 90° to both the laser and sample flow. This instrument employed two detection cells, with detection limits of ≈ 90 ppt 10 s^{-1} for NO₂ and ≈ 250 ppt 10 s^{-1} for Σ PNs, Σ ANs, and HNO₃. The lower sensitivity for higher oxides accounts for noise associated with subtraction of the up to 40 ppb NO₂ present in these experiments. Detection limits for this instrument were calculated as described by Day et al. (2002).

2.3 AMS and other particle instrumentation

An aerosol mass spectrometer (Aerodyne TOF-AMS) was operated to measure the aerosol chemical composition. The AMS was connected to the SAPHIR chamber via a stainless steel tube to minimize losses in the sampling line. The AMS working principles and modes of operation are explained in detail elsewhere (Canagartna et al., 2007). In brief, an aerodynamic lens system at the instrument inlet is used to remove gas and supermicron particles from the sample flow, while submicron particles are impacted on a tungsten vaporizer which is held at ≈ 600 °C. The resulting vapors are ionized with 70 eV electron impact ionization. A time of flight mass spectrometer is used for high resolution analysis of the chemical composition of these ions.

For the extraction of chemically resolved mass concentrations of individual species the AMS raw data are typically evaluated with standard assumptions as described by Allan et al. (2004). In brief, this approach makes use of the reproducibility of mass spectral patterns of typical inorganic aerosol components such as ammonium, sulphate and nitrate. Subtracting from a measured mass spectrum the contributions of inorganic constituents and the contribution of gas phase sample, which is exclusively composed of N₂, O₂, H₂O and gases with mixing ratios in the ppm range, one obtains the mass spectrum of the organic aerosol. Due to the non-selective ionization with electron impact at 70 eV used in the AMS and the high fragmentation induced, further identification

Secondary organic aerosol from NO₃+limonene

J. L. Fry et al.

Title Page

Abstract

Introduction

Conclusions

References

Tables

Figures

◀

▶

◀

▶

Back

Close

Full Screen / Esc

Printer-friendly Version

Interactive Discussion



**Secondary organic
aerosol from
NO₃+limonene**

J. L. Fry et al.

Title Page

Abstract

Introduction

Conclusions

References

Tables

Figures

◀

▶

◀

▶

Back

Close

Full Screen / Esc

Printer-friendly Version

Interactive Discussion



of individual molecules in a complex organic component is not possible. However, positive matrix factorization can be employed to obtain information about different chemical species (see below). Furthermore the assumptions on inorganic aerosol fragmentation patterns can be tested explicitly and revised where necessary. Inorganic nitrate from e.g., NH₄NO₃ is detected as NO⁺ (*m/z* 30) and NO₂⁺ (*m/z* 46) with a typical ratio of NO₂⁺:NO⁺ of 0.35. In the W-mode (high mass resolution) of the TOF-AMS, possible interferences on mass to charge ratios 30 (e.g., CH₂O⁺) and 46 (e.g., CH₂O₂⁺) can be identified and accounted for in the further data evaluation. This option has been used for the experiments described here to derive the nitrate content and identity of the SOA. The quantification of the nitrate content of the SOA was performed based on calibrations with NH₄NO₃ aerosol. The observed ratio of NO₂⁺:NO⁺ for SOA was 0.15 ± 0.02 which is considerably lower than 0.35 throughout the experiments indicating that the aerosol did not contain significant amounts of inorganic nitrate or nitric acid. Nitrate quantification was performed under the following assumptions: the collection efficiency of the aerosol was set to one, in agreement with previous studies on NO₃+β-pinene (Fry et al., 2009) and NO₃+isoprene (Rollins et al., 2009) SOA formation. The relative ionization efficiency (RIE) of the organics was set to 1.4 which is the standard value in AMS analysis, and the RIE of nitrate was set to 1, assuming organic nitrates are ionized equally efficiently to NH₄NO₃.

Aerosol number concentrations were measured with a Water Condensation Particle Counter (TSI WCPC model 3785). To determine aerosol wall loss rate, we use the loss rate determined by an exponential fit of the decay of CPC-measured aerosol number concentration after it has peaked 10 h into the experiment, after the second limonene injection. The peak concentration was 70 000 particles cm⁻³, after which decay was steady. This fit gives an effective aerosol loss rate of $\approx 7 \times 10^{-5} \text{ s}^{-1}$, or an effective aerosol chamber lifetime of $\approx 4 \text{ h}$.

3 Results

Figure 1 displays an overview of the NO_3 +limonene experiment. All time axes are shown in hours since the beginning of the experiment, which commenced (hour 0) at 06:00 UTC on 16 July 2007. The experiment was initiated after the SAPHIR chamber had been purged overnight with clean, dry air. At 26 min into the experiment (06:26 UTC, label A in Fig. 1), 10 ppb of limonene was introduced to the chamber by adding the appropriate volume of liquid, along with 22 ppb of NO_2 . Reactive chemistry was initiated approximately 2.5 h later (08:49 UTC, label B in Fig. 1) by the addition of NO_2 to bring the concentration up to 28 ppb along with 38 ppb of O_3 . After this point, NO_3 and N_2O_5 are produced in the chamber by the following reactions:



The sum $\text{N}_2\text{O}_5 + \text{NO}_3$ is the total NO_3 reservoir, because as NO_3 is depleted, N_2O_5 decomposes rapidly to replenish NO_3 (Reaction 3).

Both O_3 and NO_3 react with the limonene, resulting in complete consumption of limonene within 2.5 h. Gas- and aerosol-phase organic nitrates are formed immediately upon initiation of this reactive stage of the experiment, with aerosol-phase nitrates increasing markedly after oxidation of the second double bond (at approximately 5 h and 10 h for the two injections). The apparent negative alkyl nitrate observations after the first injection (around hour 3 of the experiment, Fig. 1 lower panel) are due to the subtractive measurement technique for ΣANs . Both gas- and aerosol-phase organic nitrate concentrations continue to increase after the limonene is completely consumed. Little nitric acid (≤ 2 ppb) was observed over this 24-h experiment. After the consumption of limonene, NO_3 and N_2O_5 are observed to gradually build up in the chamber, as NO_2 and O_3 continue to be present in high concentration.

Secondary organic aerosol from NO_3 +limonene

J. L. Fry et al.

[Title Page](#)[Abstract](#)[Introduction](#)[Conclusions](#)[References](#)[Tables](#)[Figures](#)[◀](#)[▶](#)[◀](#)[▶](#)[Back](#)[Close](#)[Full Screen / Esc](#)[Printer-friendly Version](#)[Interactive Discussion](#)

**Secondary organic
aerosol from
NO₃+limonene**

J. L. Fry et al.

Title Page

Abstract

Introduction

Conclusions

References

Tables

Figures

◀

▶

◀

▶

Back

Close

Full Screen / Esc

Printer-friendly Version

Interactive Discussion



Four hours following the complete consumption of limonene, the SAPHIR chamber, now containing $\approx 10 \mu\text{g m}^{-3}$ of “seed” organic aerosol, was re-charged, bringing the NO₂ concentration to 38 ppb and O₃ to 60 ppb, followed by addition of ≈ 10 ppb of limonene (14:45 UTC, label C in Fig. 1). (Note: Although 10 ppb limonene was injected, a peak of only 7 ppb was observed due to slow mixing relative to rapid oxidation. Thermal dissociation of N₂O₅ gives an instantaneous source of NO₃, such that during these first minutes, oxidation is largely NO₃ driven.) We observed immediate and sustained production of organic nitrates and aerosol, with significantly higher ultimate yields of both, compared to those after the first injection. NO₃ and N₂O₅ concentrations were again observed to build up in the chamber after the limonene had been completely consumed. Then, approximately one hour into this buildup, NO₃ and N₂O₅ decrease again for several hours, corresponding to a period where the highest organic nitrate concentrations and highest aerosol mass were observed.

4 Analysis

4.1 Organic nitrate yield

The organic nitrate yields (=branching ratio of organic nitrate channel) after oxidation of the two double bonds in limonene are different. Following each injection of limonene, two time-separated sequential increases in organic nitrate concentration were observed: the first while the limonene concentration was decreasing, and the second after all limonene precursor had reacted away. Organic nitrate formation requires NO₃ reaction, as there is not any NO in the chamber to react with RO₂. During the second increase NO₃ may be oxidizing products of either the limonene+O₃ or the limonene+NO₃ reaction. In the first oxidation step, 34% of the limonene reacted with O₃, the remainder with NO₃.

We assume that the endocyclic bond reacts with NO₃ about thirty times faster than the exocyclic double bond, based on proxy alkenes (see Sect. 5). To our knowledge,

separate rate constants for NO₃ with the two double bonds in limonene have not been measured.

The absolute organic nitrate yield of the NO₃+limonene reaction can be estimated from instantaneous changes in ΣRONO₂ signal coincident with titration of limonene.

5 The apparent nitrate yield during limonene consumption (ΔΣRONO₂/ΔLimonene) is approximately 15% for both limonene injections, but this ignores the reaction of 50% of the limonene with O₃. Hence, the initial alkyl nitrate yield from NO₃+limonene reactions alone is approximately 30%.

10 The alkyl nitrate yield (including additional nitrate production after the complete consumption of limonene) is variable between the two injections. The net alkyl nitrate formed after the first and second injections of 10 ppb limonene were 1 and 3 ppb, corresponding to overall nitrate yields of 10% and 30%, respectively; however, as discussed below, the later formation of gaseous organic nitrate is complicated.

4.2 Aerosol mass yield

15 Aerosol formation was observed after each of two limonene injections. To determine aerosol yield, we first correct the aerosol mass loading for dilution and wall losses. We then calculate the mass yield as:

$$Y = \frac{\Delta M}{\Delta \text{VOC}} \quad (1)$$

20 where ΔM is the corrected aerosol mass loading (μg m⁻³) and ΔVOC is the total reacted concentration (μg m⁻³) of limonene. The yields are determined relative to each of the two separate injections of limonene, i.e., SOA formed from the first injection is simply considered “background” aerosol for the second injection. The final SOA yields observed (Fig. 2) at the peak aerosol concentration following each injection were 25% for the first injection and 40% after the second injection, suggesting that the presence
25 in the second case of 10 μg m⁻³ of existing aerosol from the first injection enhanced partitioning to the aerosol phase.

Secondary organic aerosol from NO₃+limonene

J. L. Fry et al.

Title Page

Abstract

Introduction

Conclusions

References

Tables

Figures

◀

▶

◀

▶

Back

Close

Full Screen / Esc

Printer-friendly Version

Interactive Discussion



As seen in Eq. (1), these *mass-based* yields are calculated relative to limonene reacted. Hence, it is important in the interpretation of these yields to recall that oxidation of both double bonds in limonene adds significant additional mass to the molecule. If we assume the average molecular weight of aerosol-forming species is 250 g/mole, corresponding to limonene (C₁₀H₁₆) with addition of a nitrate group (NO₃) and hydroxyl group (OH), the yield on a per-molecule basis would be 14–22%.

Following the first limonene injection, the relative SOA yields from two generations of oxidation (the oxidation of first the endo-, then the exocyclic double bonds in limonene) can be observed (Fig. 2), separated by their differing timescale. Oxidation of the first double bond in limonene by O₃ and NO₃ results in a 10% yield of SOA. The necessity for very low volatility nucleating species in this initial aerosol formation contributed to the low mass yield; while after the second injection, products of intermediate volatility could condense onto pre-existing aerosol.

Both limonene injections show relatively low initial gas-phase nitrate yields, measured as the increase in TD-LIF observed ΣRONO₂ divided by the decrease in limonene. This indicates that NO₃-limonene reactions preferentially form the non-nitrate ketone product channels. Nevertheless, these reactions constitute an efficient pathway for SOA formation. On average, 15% of the aerosol mass is constituted of nitrate (NO₃, MW=62).

5 Interpretation

5.1 Proposed reaction mechanism

Limonene is oxidized by both NO₃ and O₃, as outlined in the mechanism shown in Fig. 3. The two double bonds in limonene allow the possibility of at least two NO₃ oxidation steps, each of which can produce an organic nitrate or non-nitrate; for simplicity we assume that the non-nitrate channel produces a ketone. This assumption is based on ketones being the highest yield non-nitrate product observed in reactions of NO₃ with

Secondary organic aerosol from NO₃+limonene

J. L. Fry et al.

Title Page

Abstract

Introduction

Conclusions

References

Tables

Figures

◀

▶

◀

▶

Back

Close

Full Screen / Esc

Printer-friendly Version

Interactive Discussion



a variety of alkenes (Table III-D-1, Calvert et al., 2000). Either double bond can also react with O_3 , the products of which have been determined in other chamber studies (Maksymiuk et al., 2009): the major O3LIM product is a C_{10} backbone with a carbonyl and a carboxyl functional group added. As the limonene backbone becomes increasingly oxidized, these products can partition to the aerosol phase, generating SOA. We construct a mechanism and use observations to constrain the poorly known parameters, including the relative rates of NO_3 oxidation of the first and second double bond, the branching ratio of organic nitrate vs. ketone formation, and the gas-aerosol partitioning of the oxidation products.

5.1.1 Gas-phase kinetics

The full reaction scheme shown above (Fig. 3) is explicitly modeled with rate constants as tabulated in Table 2. Each double bond reacts with either NO_3 or O_3 , at both first and second generations of oxidation.

In a base case model, we assume the non-specific rate constant measured for NO_3 +limonene was the rate for the faster reaction at the endocyclic double bond ($1.2 \times 10^{-11} \text{ cm}^3 \text{ molec}^{-1} \text{ s}^{-1}$ at 298 K, Calvert et al. (2000), chamber temperature ranged 294–296 K during the oxidation, so no temperature dependence was assumed). We apply the ratio of the measured rate constants for NO_3 with 2-methyl-propene ($3.1 \times 10^{-13} \text{ cm}^3 \text{ molec}^{-1} \text{ s}^{-1}$, proxy for the exocyclic double bond) to NO_3 with 2-methyl-2-butene ($9.3 \times 10^{-12} \text{ cm}^3 \text{ molec}^{-1} \text{ s}^{-1}$, proxy for the endocyclic double bond) to determine the rate of the slower reaction at the exocyclic double bond ($4.0 \times 10^{-13} \text{ cm}^3 \text{ molec}^{-1} \text{ s}^{-1}$). The measured O_3 +limonene rate of $2.0 \times 10^{-16} \text{ cm}^3 \text{ molec}^{-1} \text{ s}^{-1}$ (Calvert et al., 2000) is assumed to be the total rate constant for both double bonds, with the reaction occurring 15% of the time at exocyclic double bond and 85% of the time at the endocyclic double bond, following Leungsakul et al. (2005). Applying instead the factor of 30 between rate constants at the two double bonds derived by another recent study (Donahue et al., 2007) does not significantly

Secondary organic aerosol from NO_3 +limonene

J. L. Fry et al.

Title Page

Abstract

Introduction

Conclusions

References

Tables

Figures

◀

▶

◀

▶

Back

Close

Full Screen / Esc

Printer-friendly Version

Interactive Discussion



affect results; essentially only the major product channel influences subsequent chemistry in either case. Reactions of O_3 or NO_3 with first-generation oxidation products of limonene are assumed to proceed at the same rate as on limonene itself, i.e., oxidation of one double bond does not affect rate constants at the other double bond. This is in contrast to recent studies on isoprene nitrates (Lockwood et al., 2010), which found that the nitrate group β to the double bond increased its reaction rate with O_3 . Since in this case the double bonds are separated by three bonds, we assume the effect is negligible.

The reaction of NO_3 with aldehydes produced in early generations of the chemistry are also important. The rate constants used here are estimated based on a comprehensive study of the kinetics of NO_3 reaction with a series of aldehydes (D'Anna et al., 2001).

Wall loss rates of reactive species are determined from the timescale of NO_3 , O_3 , and N_2O_5 loss in an earlier VOC-free chamber experiment, and aerosol loss rates from observed particle number density decay during this experiment. Values for the branching ratios for nitrate versus ketone production at each NO_3 oxidation step are assumed to be independent of other functional groups on the molecule. The organic nitrate branching ratios are estimated to be 32% at the exo double bond and 14% at the endo double bond, based on overall nitrate branching ratios for α - and β -pinene in the Master Chemical Mechanism v3.1 (Saunders et al., 2003).

In this base case model, NO_3 and N_2O_5 are always underpredicted, while organic nitrate is initially over predicted (after the first limonene addition, hours 4–7) and later under-predicted (hours 9–24). The model/measurement discrepancy is improved by systematically adjusting a number of the parameters in the gas phase mechanism, subject to observational constraints, which are summarized in Table 1.

Since the concentrations of NO_3 and N_2O_5 are determined by their source (R1) and sinks, and the source is well constrained, we adjust the modeled NO_3 sinks to find the best agreement between modeled and measured NO_3 and N_2O_5 after limonene has fully reacted after the first injection (hours 4–7, Fig. 4). The primary sinks of NO_3 are

Secondary organic aerosol from NO_3 +limonene

J. L. Fry et al.

Title Page

Abstract

Introduction

Conclusions

References

Tables

Figures

⏪

⏩

◀

▶

Back

Close

Full Screen / Esc

Printer-friendly Version

Interactive Discussion



reaction with limonene and its oxidation products. We find the best agreement using rate constants for NO₃ with limonene and its oxidation products that are a factor of two lower than the literature value (Calvert et al., 2000).

During the first limonene oxidation event, consumption of limonene by O₃ was appreciable relative to NO₃ oxidation (approximately 25% of the limonene is consumed by ozone), since the O₃ was injected after limonene and therefore the NO₃+limonene reaction was limited by the NO₃ production rate. We observe organic nitrate products to appear immediately in both gas and aerosol phase.

Finally, we tune the unknown rate constant of the larger aldehydes formed in the oxidation mechanism, TRIKET, G2O3 and DIKETONO3, with NO₃ using the total HNO₃ produced in the experiment (≈2 ppb) as a constraint, since these are the sole sources of nitric acid. We find the rate of NO₃+TRIKET or DIKETONO3 to be 50 times the rate of NO₃+HCHO, a reasonable range for a larger aldehyde (D'Anna et al., 2001).

These three constraints result in gas-phase chemistry that reproduces the concentrations after the first limonene injection reasonably well (Fig. 4). However, we note that the model overestimates NO₃ and that the second pulse of aerosol nitrate is overpredicted by about 30% before the second limonene injection (at hour 9).

5.1.2 Modeling aerosol partitioning of condensing species

We model the gas-aerosol partitioning of the limonene oxidation products using the equilibrium absorptive partitioning formalism, following Pankow and Capouet (Pankow, 1994; Capouet and Muller, 2006):

$$K_p = \frac{F/TSP}{A} = \frac{760 \cdot R \cdot T \cdot f_{om}}{MW_{om} \cdot 10^6 \cdot \zeta \cdot p_{vap}} \quad (2)$$

F and A are the total aerosol-phase and gaseous concentrations of the compound of interest, and TSP is the concentration of total suspended particulate matter. In the second expression showing the equilibrium constant in terms of thermodynamic properties, R is the universal gas constant

Secondary organic aerosol from NO₃+limonene

J. L. Fry et al.

Title Page

Abstract

Introduction

Conclusions

References

Tables

Figures

◀

▶

◀

▶

Back

Close

Full Screen / Esc

Printer-friendly Version

Interactive Discussion



($8.314 \text{ J mol}^{-1} \text{ K}^{-1} = 8.206 \times 10^{-5} \text{ atm m}^3 \text{ K}^{-1} \text{ mol}^{-1}$), T is temperature (K), f_{om} is the weight fraction of organic matter in the total aerosol (=1 for these experiments), MW_{om} is the average molecular weight of the absorbing organic material (g mol^{-1}), ζ is the activity coefficient of the compound of interest in the condensed phase (assumed=1 for these experiments), and p_{vap} is the subcooled vapor pressure of the compound of interest (Torr); 760 (Torr atm^{-1}) and 10^6 ($\mu\text{g g}^{-1}$) are conversion factors. This gives K_p in units of $\text{m}^3 \mu\text{g}^{-1}$.

We explicitly model the equilibrium gas/aerosol partitioning of 11 condensable species: EXONO3/ENDONO3 (same p_{vap}), DINO3, KETONO3/O3LIM2NO3 (same p_{vap}), DIKETONO3/O3LIMNO3 (same p_{vap}), TRIKET, G2O3, and O3LIM/O3LIM2 (same p_{vap} assumed for O_3 product from either double bond). For each, we calculate p_{vap} based on the proposed product structures shown in Fig. 3 and the group contribution method of Pankow and Asher (2008). These calculated values and the tuned values used in the present model are reported in Table 3. To initiate aerosol formation, a small amount of “seed” aerosol is injected in the model at the moment of ozone injection into the limonene; the seed does not affect ultimate aerosol yield in this equilibrium model. Partitioning is implemented by determining the gas-phase and aerosol fractions of each species at each time step, assuming that this partitioning is effectively instantaneous.

As has been noted in previous studies (Leungsakul et al., 2005; Fry et al., 2009), the predicted vapor pressures underestimates the aerosol produced. This suggests that the actual structures of limonene oxidation products are either more oxidized or oligomerized forms of the proposed structures, or that the group contribution method overestimates vapor pressure.

We employ the observed mass loading of organic and nitrate aerosol from the AMS as well as the observed gas/aerosol partitioning of organic nitrate after the first limonene injection as constraints to determine tuning factors to apply to the p_{vap} 's in the model. The shape of the time trace allows distinction between first- and

**Secondary organic
aerosol from
 NO_3 +limonene**

J. L. Fry et al.

Title Page

Abstract

Introduction

Conclusions

References

Tables

Figures

◀

▶

◀

▶

Back

Close

Full Screen / Esc

Printer-friendly Version

Interactive Discussion



second-generation oxidation products. Measurement/model agreement on the organic and nitrate aerosol loading before and after tuning vapor pressures are shown in Fig. 5. After determining the tuning factors that best approximate the experimental data, the same group contribution method can be used to rationalize those factors applied. Most striking is the need for both first- and second-generation NO₃ products to have significantly lower volatility. For example, the shift in DIKETONO₃'s vapor pressure could be caused by adding two carbonyl groups to the backbone. Two carbonyls lower the vapor pressure roughly half as much as one hydroxyl group. This high degree of oxidation is consistent with recent work on the ozone/limonene system (Bateman et al., 2009).

Initially, only one-fifth the observed aerosol nitrate after the first limonene injection was produced in the model. The vapor pressures were fit to the first nine hours of observed gas and aerosol phase nitrates, greatly improving measurement/model agreement (Fig. 4). This is a function both of the reduced vapor pressures of the nitrates themselves, and of having in general more organic aerosol mass onto which organic nitrates can partition.

5.2 Interpreting nitrate and aerosol formation after second limonene injection

Kinetic modeling captures limonene consumption by NO₃ and O₃, initial alkyl nitrate yields, overall aerosol yield and organic to nitrate ratio of the aerosol produced. However, the agreement between model and experimental observations of NO₃ shown in Fig. 4 does not persist through the second limonene injection. Without further changes, the gas-phase organic nitrate from hour 10 onwards is drastically underpredicted, while NO₃ is overpredicted. Because the maximum discrepancy coincides with the highest aerosol loading, reaction of NO₃ on the surface of the organic aerosol to produce an RONO₂ species that is more volatile than its parent aerosol-bound VOC is suggested. We model the aerosol uptake of NO₃ using:

$$k_{\text{uptake}} = \frac{\gamma v_{\text{NO}_3} SA}{4} \quad (3)$$

Secondary organic aerosol from NO₃+limonene

J. L. Fry et al.

Title Page

Abstract

Introduction

Conclusions

References

Tables

Figures

◀

▶

◀

▶

Back

Close

Full Screen / Esc

Printer-friendly Version

Interactive Discussion



Secondary organic aerosol from NO₃+limonene

J. L. Fry et al.

Title Page

Abstract

Introduction

Conclusions

References

Tables

Figures

◀

▶

◀

▶

Back

Close

Full Screen / Esc

Printer-friendly Version

Interactive Discussion



where γ is the unitless uptake coefficient, v_{NO_3} is the molecular speed of NO_3 (cm s^{-1}), and SA is the total aerosol surface area per volume ($\text{cm}^2 \text{cm}^{-3}$) calculated from the modeled aerosol mass, assumed density (1.6 g cm^{-3} , Fry et al., 2009) and measured mode particle radius (AMS). For the purposes of this modeling, we assume the limiting case: that every organic nitrate produced by this reaction evaporates to the gas phase. We multiply SA by the (modeled) fraction of aerosol containing unsaturated double bonds to more easily enable comparison to uptake measurements on well-defined hydrocarbon surfaces. With the observed and modeled aerosol surface area peaking at $1.3 \times 10^{-6} \text{ cm}^2 \text{cm}^{-3}$, an uptake coefficient of NO_3 onto the fraction of the aerosol that contains double bonds of $\gamma \approx 5 \times 10^{-1}$ provides the best fit to the gas/aerosol nitrate partitioning after the 2nd limonene injection (Fig. 6). This uptake coefficient was determined using observed NO_3 ; the figure shows the resulting improvement of fit in the full model using this γ . In this experiment, the double-bond containing fraction of the aerosol ranges between 10% and 40%, meaning the uptake coefficient on the total aerosol formed in the SAPHIR chamber ranged between $\gamma = 0.05$ – 0.2 .

This value of uptake coefficient is in general agreement with the results of Gross and Bertram (2009), who measured uptake coefficients around 2×10^{-3} on neat liquid surfaces of saturated ethers and polyols, up to 2×10^{-1} for a mono-unsaturated carboxylic acid. Under the dry conditions of the present experiment, heterogeneous uptake of N_2O_5 was expected to be negligible. In our previous study on SOA formation from $\text{NO}_3 + \beta$ -pinene (Fry et al., 2009), we found that we did not need to include any heterogeneous chemistry to explain observations. This is reasonable, since in that study the aerosol formed by NO_3 reaction with the monounsaturated alkene would not have contained double bonds. Given the low aerosol surface area in that study and using the measured uptake coefficient for NO_3 on saturated alkanes of around 10^{-3} (Gross and Bertram, 2009; Moise et al., 2002), the heterogeneous loss rate of NO_3 was negligibly small. In contrast, in this limonene experiment the aerosol contains some unsaturated double bonds, leading to a higher uptake coefficient and significant heterogeneous NO_3 uptake.

**Secondary organic
aerosol from
NO₃+limonene**

J. L. Fry et al.

Title Page

Abstract

Introduction

Conclusions

References

Tables

Figures

◀

▶

◀

▶

Back

Close

Full Screen / Esc

Printer-friendly Version

Interactive Discussion



Given the underpredicted aerosol formation from our raw reaction mechanism, this model is almost certainly incomplete in terms of later oxidation steps. Therefore, it is possible that a late-peaking gas-phase species is instead responsible for this very efficient observed conversion of NO₃ to volatile organic nitrate; however, as will be shown below, there is additional evidence in the AMS data for consumption of organic aerosol that bolsters this hypothesis of heterogeneous NO₃ reactions.

Despite the improvement in modeling gas/aerosol partitioning of organic nitrate with this heterogeneous process included, no reasonable permutations on the rate constants or partitioning constants of mechanism described thus far can fully reproduce the major unique feature of this “second experiment”: the pronounced dip in NO₃ and N₂O₅ around 12 h. Figure 7 shows the measured and modeled NO₃ and N₂O₅ with the complete model described here. A slight dip appears due to the heterogeneous uptake of NO₃, but not nearly as abrupt nor with as dramatic a recovery as observed in the data. We have attempted increasing the rate of that process, as well as all other NO₃ sinks in the present mechanism. In all cases, this further depletes NO₃/N₂O₅ everywhere rather than simply deepening the dip. What appears to be necessary is a chemical process that is activated only at hour 11 and ceases at hour 13. This remains a major gap in the modeling of this system, which we have not been able to resolve with the mechanism described here.

Table 1 summarizes all tuned parameters in the gas and aerosol model and the observations used to constrain each.

5.3 Aerosol chemical composition

As in previous investigations of the SOA formation from reactions of NO₃ with biogenic VOCs (β -pinene, Fry et al. (2009) and isoprene, Rollins et al. (2009)), the main characteristic feature of the organic nitrates is a low NO⁺/NO₂⁺ ratio. In addition, the *m/z* 76 (CH₂NO₃⁺) ion fragment again appears as an indicator for the presence of organic nitrates. Beyond this, the AMS observations diverge from previous experiments somewhat. Here, a heavier *m/z* 184 (C₉H₁₄NO₃⁺) fragment is clearly present throughout

the experiment (Fig. 8). The increase in this fragment over the course of the experiment suggests that larger nitrates are incorporated into the aerosol via later-generation chemistry.

In order to further assess SOA chemistry (ozonolysis versus NO_3 oxidation sources, first versus second generation oxidation), the AMS organic aerosol fraction was analysed using positive matrix factorization (PMF) (Paatero and Tapper, 1994; Paatero, 1997). This analysis was performed entirely independent of the above described kinetics modeling. The PMF analysis applied principles and utilized code as introduced by Ulbrich et al. (2009). The number of factors used to describe the total aerosol formed was selected based on the residuals both in MS and time space. Since the sources for aerosol formation were reactions of limonene with NO_3 and O_3 , the nitrate that was observed in the course of the experiment was included in the PMF analysis. Three factors were found to describe the measured data with residuals below 2% at all times (Fig. 9).

The resolved PMF components (Fig. 10) can be interpreted based upon the correlation of their time derivatives with rates of selected processes based on modeled species. Factor 1 has high nitrate content (m/z 30 and 46 contribute 12% to the factor 1 mass), and the ratio of 46/30 is 0.13, well below the typical ratio observed for NH_4NO_3 . It is also correlated to the AMS measured nitrate ($R^2=0.95$) and is thus interpreted as organic nitrate. Of the modeled organic nitrate production rates, factor 1 correlates poorly with first-generation production ($[\text{NO}_3] \times [\text{LIM}]$, $R^2=0.46$), but correlates well with second-generation production from ozone oxidation of first generation nitrates ($[\text{O}_3] \times [\text{ENDONO}_3]$, $R^2=0.83$). It is not at all correlated with NO_3 oxidation of first-generation ozone products.

The second factor is better correlated with first-generation ozone oxidation of limonene ($[\text{O}_3] \times [\text{LIM}]$, $R^2=0.73$) than second-generation ($[\text{O}_3] \times [\text{O}_3\text{LIM}]$, $R^2=0.26$). Its mass spectral pattern supports the interpretation of oxidized organics from the first generation reaction of O_3 with limonene.

Secondary organic aerosol from NO_3 +limonene

J. L. Fry et al.

[Title Page](#)[Abstract](#)[Introduction](#)[Conclusions](#)[References](#)[Tables](#)[Figures](#)[⏪](#)[⏩](#)[◀](#)[▶](#)[Back](#)[Close](#)[Full Screen / Esc](#)[Printer-friendly Version](#)[Interactive Discussion](#)

**Secondary organic
aerosol from
NO₃+limonene**

J. L. Fry et al.

[Title Page](#)[Abstract](#)[Introduction](#)[Conclusions](#)[References](#)[Tables](#)[Figures](#)[⏪](#)[⏩](#)[◀](#)[▶](#)[Back](#)[Close](#)[Full Screen / Esc](#)[Printer-friendly Version](#)[Interactive Discussion](#)

The third component also contains significant organic nitrate: the ratio of 46/30 is 0.17 for factor 3 and the sum of 30 and 46 contribute 19% of the total mass of this factor. It is best correlated with reaction of NO₃ with ozone-produced aerosol ([NO₃]×[O3LIMaero], $R^2=0.73$). A correlation almost as good is found using [NO₃]×SA, weighted by factor 2 ($R^2=0.61$), which was attributed to the purely ozone-generated aerosol. We therefore interpret factor 3 as representing heterogeneous uptake processes on the SOA in the second part of the experiment. The decay of the organic factor 2 coincident with increase in this factor also supports this interpretation. It is possible that NO₃ uptake onto limonene SOA results sometimes in revolatilization of an organic nitrate (as invoked in this model), sometimes in net uptake of nitrate, creating larger multifunctional nitrates which remain in the aerosol phase, and sometimes in NO₂ release and chemical conversion of the aerosol phase.

6 Conclusions

Observations of the reaction of NO₃ with limonene show that the RONO₂ yield is approximately 30%, implying significant release of the nitrate functional group after attack at the double bonds. The aerosol mass yield is 25–40%. We find that aerosol composition is affected by NO₃ reaction with increased incorporation of organic nitrate into the aerosol over time and apparent conversion of aerosol bound alkene moieties to nitrate moieties. These conclusions bolster other recent evidence suggesting that nitrate addition to monoterpenes may be an important player in the aerosol budget in those locations where biogenic terpene emissions are large and NO_x is abundant.

Acknowledgements. The Berkeley authors were supported by NSF ATM-0639847 and NSF ATM-0511829. The authors thank the entire SAPHIR NO₃ intercomparison campaign team, June 2007 at Forschungszentrum Jülich, for their support of these experiments. This work was a joint activity of the European Network of Excellence ACCENT (contract no: GOCE CT-2004-505337) and EUROCHAMP.

References

- Allan, J., Delia, A., Coe, H., Bower, K., Alfarra, M., Jimenez, J., Middlebrook, A., Drewnick, F., Onasch, T., Canagaratna, M., Jayne, J., and Worsnop, D.: A generalised method for the extraction of chemically resolved mass spectra from aerodyne aerosol mass spectrometer data, *J. Aerosol Sci.*, 35, 909–922, 2004. 31088
- 5 Apel, E. C., Brauers, T., Koppmann, R., Bandowe, B., Boßmeyer, J., Holzke, C., Tillmann, R., Wahner, A., Wegener, R., Brunner, A., Jocher, M., Ruuskanen, T., Spirig, C., Steigner, D., Steinbrecher, R., Gomez Alvarez, E., Müller, K., Burrows, J. P., Schade, G., Solomon, S. J., Ladstätter-Weißmayer, A., Simmonds, P., Young, D., Hopkins, J. R., Lewis, A. C.,
- 10 Legreid, G., Reimann, S., Hansel, A., Wisthaler, A., Blake, R. S., Ellis, A. M., Monks, P. S., and Wyche, K. P.: Intercomparison of oxygenated volatile organic compound measurements at the SAPHIR atmosphere simulation chamber, *J. Geophys. Res.*, 113, D20307, doi:10.1029/2008JD009865, 2008. 31086
- Apodaca, R., Dorn, H.-P., Ball, S. M., Brauers, T., Brown, S. S., Cohen, R. C., Crowley, J.,
- 15 Dorn, H.-P., D. W., Fry, J. L., Fuchs, H., Haseler, R., Heitmann, U., Kato, S., Kajii, Y., Kiendler-Scharr, A., Kleffmann, J., Labazan, I., Matsumoto, J., Nishida, S., Rollins, A. W., Tillmann, R., Wahner, A., Wegener, R., Wooldridge, P. J., and Simpson, W. R.: Intercomparison of N₂O₅ sensors using SAPHIR reaction chamber, *Atmos. Chem. Phys.*, in preparation, 2010. 31086, 31087
- 20 Bateman, A. P., Nizkorodov, S. A., Laskin, J., and Laskin, A.: Time-resolved molecular characterization of limonene/ozone aerosol using high-resolution electrospray ionization mass spectrometry, *Phys. Chem. Chem. Phys.*, 11, 7931–7942, doi^{10.1039/b905288g}, 2009. 31098
- Bohn, B. and Zilken, H.: Model-aided radiometric determination of photolysis frequencies in a sunlit atmosphere simulation chamber, *Atmos. Chem. Phys.*, 5, 191–206, doi:10.5194/acp-5-191-2005, 2005. 31086
- 25 Calvert, J., Atkinson, J., Kerr, J., Madronich, S., Moortgat, G. K., Wallington, T., and Yarwood, G.: Mechanisms of the atmospheric oxidation of the alkenes, Oxford University Press, New York, NY, 2000. 31094, 31096
- 30 Canagaratna, M., Jayne, J., Jimenez, J., Allan, J., Alfarra, M., Zhang, Q., Onasch, T., Drewnick, F., Coe, H., Middlebrook, A., Delia, A., Williams, L., Trimborn, A., Northway, M., DeCarlo, P., Kolb, C., Davidovits, P., and Worsnop, D.: Chemical and microphysical character-

Secondary organic aerosol from NO₃+limonene

J. L. Fry et al.

Title Page

Abstract

Introduction

Conclusions

References

Tables

Figures



Back

Close

Full Screen / Esc

Printer-friendly Version

Interactive Discussion



**Secondary organic
aerosol from
NO₃+limonene**

J. L. Fry et al.

Title Page

Abstract

Introduction

Conclusions

References

Tables

Figures

◀

▶

◀

▶

Back

Close

Full Screen / Esc

Printer-friendly Version

Interactive Discussion



riation of ambient aerosols with the aerodyne aerosol mass spectrometer, *Mass Spectrom. Rev.*, 26, 185–222, 2007. 31088

Capouet, M. and Mller, J.-F.: A group contribution method for estimating the vapour pressures of α -pinene oxidation products, *Atmos. Chem. Phys.*, 6, 1455–1467, doi:10.5194/acp-6-1455-2006, 2006. 31096

D'Anna, B., Andresen, O., Gefen, Z., and Nielsen, C. J.: Kinetic study of OH and NO₃ radical reactions with 14 aliphatic aldehydes, *Phys. Chem. Chem. Phys.*, 3, 3057–3063, 2001. 31095, 31096

Day, D. A., Wooldridge, P. J., Dillon, M., Thornton, J. A., and Cohen, R. C.: A thermal dissociation laser-induced fluorescence instrument for in situ detection of NO₂, peroxy nitrates, alkyl nitrates, and HNO₃, *J. Geophys. Res.*, 107(D6), 4046, doi:10.1029/2001JD000779, 2002. 31087

de Gouw, J. A., Middlebrook, A. M., Warneke, C., Goldan, P. D., Kuster, W. C., Roberts, J. M., Fehsenfeld, F. C., Worsnop, D. R., Canagaratna, M. R., Pszenny, A. A. P., Keene, W. C., Marchewka, M., Bertman, S. B., and Bates, T. S.: Budget of organic carbon in a polluted atmosphere: results from the New England Air Quality Study in 2002, *J. Geophys. Res.-Atmos.*, 110, D16305, doi:10.1029/2004JD005623, 2005. 31085

Donahue, N. M., Tischuk, J. E., Marquis, B. J., and Huff Hartz, K. E.: Secondary organic aerosol from limona ketone: insights into terpene ozonolysis via synthesis of key intermediates, *Phys. Chem. Chem. Phys.*, 9, 2991–2998, doi:10.1039/b701333g, 2007. 31094

Dorn, H. P., Apodaca, R., Ball, S., Brauers, T., Brown, S. S., Cohen, R. C., Crowley, J., Dube, W. P., Fry, J., Fuchs, H., Haseler, R., Heitmann, U., Jones, R., Kato, S., Kajii, Y., Kiendler-Scharr, A., Labazan, I., Matsumoto, J., Meinen, J., Nishida, S., Platt, U., Rohrer, F., Rollins, A., Ruth, A., Schlosser, E., Schuster, G., Shillings, A., Simpson, W., Thieser, J., Tillmann, R., Varma, R., Venables, D., Wahner, A., Wegener, R., and Wooldridge, P. J.: Intercomparison of 10 different NO₃ measurement techniques at the simulation chamber SAPHIR, *Atmos. Chem. Phys.*, in preparation, 2010. 31086, 31087

Dube, W. P., Brown, S. S., Osthoff, H. D., Nunley, M. R., Circiora, S. J., Paris, M. W., McLaughlin, R. J., and Ravishankara, A. R.: Aircraft instrument for simultaneous, in situ measurement of NO₃ and N₂ O₅ via pulsed cavity ring-down spectroscopy, *Rev. Sci. Instrum.*, 77, 2006. 31087

Eerdeken, G., Yassaa, N., Sinha, V., Aalto, P. P., Aufmhoff, H., Arnold, F., Fiedler, V., Kulmala, M., and Williams, J.: VOC measurements within a boreal forest during spring 2005: on

**Secondary organic
aerosol from
NO₃+limonene**

J. L. Fry et al.

Title Page

Abstract

Introduction

Conclusions

References

Tables

Figures

◀

▶

◀

▶

Back

Close

Full Screen / Esc

Printer-friendly Version

Interactive Discussion



the occurrence of elevated monoterpene concentrations during night time intense particle concentration events, *Atmos. Chem. Phys.*, 9, 8331–8350, doi:10.5194/acp-9-8331-2009, 2009. 31084

5 Fry, J. L., Kiendler-Scharr, A., Rollins, A. W., Wooldridge, P. J., Brown, S. S., Fuchs, H., Dubé, W., Mensah, A., dal Maso, M., Tillmann, R., Dorn, H.-P., Brauers, T., and Cohen, R. C.: Organic nitrate and secondary organic aerosol yield from NO₃ oxidation of β -pinene evaluated using a gas-phase kinetics/aerosol partitioning model, *Atmos. Chem. Phys.*, 9, 1431–1449, doi:10.5194/acp-9-1431-2009, 2009. 31089, 31097, 31099, 31100, 31111

10 Fuchs, H., Dubé, W., Ciciora, S., and Brown, S.: Determination of inlet transmission and conversion efficiencies for in situ measurements of the nocturnal nitrogen oxides, NO₃, N₂O₅ and NO₂ via pulsed cavity ring-down spectroscopy, *Anal. Chem.*, 80, 6010–6017, 2008. 31087

15 Fuchs, H., Ball, S. M., Bohn, B., Brauers, T., Cohen, R. C., Dorn, H.-P., Dubé, W. P., Fry, J. L., Häsel, R., Heitmann, U., Jones, R. L., Kleffmann, J., Mentel, T. F., Müsgen, P., Rohrer, F., Rollins, A. W., Ruth, A. A., Kiendler-Scharr, A., Schlosser, E., Shillings, A. J. L., Tillmann, R., Varma, R. M., Venables, D. S., Villena Tapia, G., Wahner, A., Wegener, R., Wooldridge, P. J., and Brown, S. S.: Intercomparison of measurements of NO₂ concentrations in the atmosphere simulation chamber SAPHIR during the NO₃Comp campaign, *Atmos. Meas. Tech.*, 3, 21–37, doi:10.5194/amt-3-21-2010, 2010. 31086

20 Goldstein, A. H. and Galbally, I. E.: Known and unexplored organic constituents in the Earth's atmosphere, *Environ. Sci. Technol.*, 41, 1515–1521, 2007. 31084

Griffin, R. J., Cocker, D. R., Flagan, R. C., and Seinfeld, J. H.: Organic aerosol formation from the oxidation of biogenic hydrocarbons, *J. Geophys. Res.-Atmos.*, 104, 3555–3567, 1999. 31084

Gross, S. and Bertram, A.: Personal communication, 2009. 31099

25 Guenther, A., Hewitt, C. N., Erickson, D., Fall, R., Geron, C., Graedel, T., Harley, P., Klinger, L., Lerdau, M., McKay, W. A., Pierce, T., Scholes, B., Steinbrecher, R., Tallamraju, R., Taylor, J., and Zimmerman, P.: A global model of natural volatile organic compound emissions, *J. Geophys. Res.*, 100, 8873–8892, doi:10.1029/94JD02950, 1995. 31084

30 Hallquist, M., Wangberg, I., Ljungstrom, E., Barnes, I., and Becker, K. H.: Aerosol and product yields from NO₃ radical-initiated oxidation of selected monoterpenes, *Environ. Sci. Technol.*, 33, 553–559, 1999. 31084

Lane, T. E., Donahue, N. M., and Pandis, S. N.: Simulating secondary organic aerosol formation using the volatility basis-set approach in a chemical transport model, *Atmos. Environ.*, 42,

Secondary organic aerosol from NO₃+limonene

J. L. Fry et al.

Title Page

Abstract

Introduction

Conclusions

References

Tables

Figures

◀

▶

◀

▶

Back

Close

Full Screen / Esc

Printer-friendly Version

Interactive Discussion



7439–7451, doi:10.1016/j.atmosenv.2008.06.026, 2008. 31085

Leungsakul, S., Jaoui, M., and Kamens, R.: Kinetic mechanism for predicting secondary organic aerosol formation from the reaction of d-limonene with ozone, *Environ. Sci. Technol.*, 39, 9583–9594, doi:10.1021/es0492687, 2005. 31094, 31097

5 Lindinger, W., Hansel, A., and Jordan, A.: Proton-transfer-reaction mass spectrometry (PTR-MS): on-line monitoring of volatile organic compounds at pptv levels, *Chem. Soc. Rev.*, 27, 347–354, 1998. 31086

Lockwood, A. L., Shepson, P. B., Fiddler, M. N., and Alaghmand, M.: Isoprene nitrates: preparation, separation, identification, yields, and atmospheric chemistry, *Atmos. Chem. Phys.*, 10, 6169–6178, doi:10.5194/acp-10-6169-2010, 2010. 31095

10 Maksymiuk, C. S., Gayahtri, C., Gil, R. R., and Donahue, N. M.: Secondary organic aerosol formation from multiphase oxidation of limonene by ozone: mechanistic constraints via two-dimensional heteronuclear NMR spectroscopy, *Phys. Chem. Chem. Phys.*, 11, 7810–7818, doi:10.1039/b820005j, 2009. 31085, 31094

15 Moise, T., Talukdar, R. K., Frost, G. J., Fox, R. W., and Rudich, Y.: Reactive uptake of NO₃ by liquid and frozen organics, *J. Geophys. Res.*, 107(D2), 6–1, doi:10.1029/2001JD000334, 2002. 31099

Paatero, P.: Least squares formulation of robust non-negative factor analysis, *Chemometr. Intell. Lab.*, 37, 23–35, 1997. 31101

20 Paatero, P. and Tapper, U.: Positive matrix factorization – a nonnegative factor model with optimal utilization of error-estimates of data values, *Environmetrics*, 5, 111–126, 1994. 31101

Pankow, J. F.: An absorption-model of gas-particle partitioning of organic-compounds in the atmosphere, *Atmos. Environ.*, 28, 185–188, 1994. 31096

25 Pankow, J. F. and Asher, W. E.: SIMPOL.1: a simple group contribution method for predicting vapor pressures and enthalpies of vaporization of multifunctional organic compounds, *Atmos. Chem. Phys.*, 8, 2773–2796, doi:10.5194/acp-8-2773-2008, 2008. 31097, 31111

Pye, H. O. T., Chan, A. W. H., Barkley, M. P., and Seinfeld, J. H.: Global modeling of organic aerosol: the importance of reactive nitrogen (NO_x and NO₃), *Atmos. Chem. Phys.*, 10, 11261–11276, doi:10.5194/acp-10-11261-2010, 2010. 31085

30 Quinn, P. K., Bates, T. S., Coffman, D., Onasch, T. B., Worsnop, D., Baynard, T., de Gouw, J. A., Goldan, P. D., Kuster, W. C., Williams, E., Roberts, J. M., Lerner, B., Stohl, A., Pettersson, A., and Lovejoy, E. R.: Impacts of sources and aging on submicrometer aerosol properties in the marine boundary layer across the Gulf of Maine, *J. Geophys. Res.*, 111, D23S36,

doi:10.1029/2006JD007582, 2006. 31085

Ridley, B., Grahek, F., and Walega, J.: A small, high-sensitivity, medium-response ozone detector suitable for measurements from light aircraft, *J. Atmos. Ocean Tech.*, 9, 142–148, 1992. 31086

5 Rohrer, F., Bohn, B., Brauers, T., Brüning, D., Johnen, F.-J., Wahner, A., and Kleffmann, J.: Characterisation of the photolytic HONO-source in the atmosphere simulation chamber SAPHIR, *Atmos. Chem. Phys.*, 5, 2189–2201, doi:10.5194/acp-5-2189-2005, 2005. 31086

Rollins, A. W., Kiendler-Scharr, A., Fry, J. L., Brauers, T., Brown, S. S., Dorn, H.-P., Dubé, W. P., Fuchs, H., Mensah, A., Mentel, T. F., Rohrer, F., Tillmann, R., Wegener, R., Wooldridge, P. J., and Cohen, R. C.: Isoprene oxidation by nitrate radical: alkyl nitrate and secondary organic aerosol yields, *Atmos. Chem. Phys.*, 9, 6685–6703, doi:10.5194/acp-9-6685-2009, 2009. 31089, 31100

Sakulyanontvittaya, T., Duhl, T., Wiedinmyer, C., Helmig, D., Matsunaga, S., Potosnak, M., Milford, J., and Guenther, A.: Monoterpene and sesquiterpene emission estimates for the United States, *Environ. Sci. Technol.*, 42, 1623–1629, doi:10.1021/es702274e, 2008. 31085

15 Saunders, S. M., Jenkin, M. E., Derwent, R. G., and Pilling, M. J.: Protocol for the development of the Master Chemical Mechanism, MCM v3 (Part A): tropospheric degradation of non-aromatic volatile organic compounds, *Atmos. Chem. Phys.*, 3, 161–180, doi:10.5194/acp-3-161-2003, 2003. 31095

20 Schichtel, B., Malm, W., Bench, G., Fallon, S., McDade, C., Chow, J., and Watson, J.: Fossil and contemporary fine particulate carbon fractions at 12 rural and urban sites in the United States, *J. Geophys. Res.*, 113, doi:10.1029/2007JD008605, 2008. 31085

Schlosser, E., Brauers, T., Dorn, H.-P., Fuchs, H., Häseler, R., Hofzumahaus, A., Holland, F., Wahner, A., Kanaya, Y., Kajii, Y., Miyamoto, K., Nishida, S., Watanabe, K., Yoshino, A., Kubistin, D., Martinez, M., Rudolf, M., Harder, H., Berresheim, H., Elste, T., Plass-Dülmer, C., Stange, G., and Schurath, U.: Technical Note: Formal blind intercomparison of OH measurements: results from the international campaign HOxComp, *Atmos. Chem. Phys.*, 9, 7923–7948, doi:10.5194/acp-9-7923-2009, 2009. 31086

30 Slowik, J. G., Stroud, C., Bottenheim, J. W., Brickell, P. C., Chang, R. Y.-W., Liggio, J., Makar, P. A., Martin, R. V., Moran, M. D., Shantz, N. C., Sjostedt, S. J., van Donkelaar, A., Vlasenko, A., Wiebe, H. A., Xia, A. G., Zhang, J., Leaitch, W. R., and Abbatt, J. P. D.: Characterization of a large biogenic secondary organic aerosol event from eastern Canadian forests, *Atmos. Chem. Phys.*, 10, 2825–2845, doi:10.5194/acp-10-2825-2010, 2010. 31084

Secondary organic aerosol from NO₃+limonene

J. L. Fry et al.

Title Page

Abstract

Introduction

Conclusions

References

Tables

Figures

◀

▶

◀

▶

Back

Close

Full Screen / Esc

Printer-friendly Version

Interactive Discussion



**Secondary organic
aerosol from
NO₃+limonene**

J. L. Fry et al.

Title Page

Abstract

Introduction

Conclusions

References

Tables

Figures

◀

▶

◀

▶

Back

Close

Full Screen / Esc

Printer-friendly Version

Interactive Discussion



- Spittler, M., Barnes, I., Bejan, I., Brockmann, K. J., Benter, T., and Wirtz, K.: Reactions of NO₃ radicals with limonene and alpha-pinene: product and SOA formation, *Atmos. Environ.*, 40, S116–S127, doi:10.1016/j.atmosenv.2005.09.093, 2006. 31085
- Thornton, J. A., Wooldridge, P. J., and Cohen, R. C.: Atmospheric NO₂: in situ laser-induced fluorescence detection at parts per trillion mixing ratios, *Anal. Chem.*, 72, 528–539, 2000. 31087
- Tunved, P., Hansson, H., Kerminen, V., Strom, J., Dal Maso, M., Lihavainen, H., Viisanen, Y., Aalto, P., Komppula, M., and Kulmala, M.: High natural aerosol loading over boreal forests, *Science*, 312, 261–263, doi:10.1126/science.1123052, 2006. 31084
- Ulbrich, I. M., Canagaratna, M. R., Zhang, Q., Worsnop, D. R., and Jimenez, J. L.: Interpretation of organic components from Positive Matrix Factorization of aerosol mass spectrometric data, *Atmos. Chem. Phys.*, 9, 2891–2918, doi:10.5194/acp-9-2891-2009, 2009. 31101
- Wainman, T., Zhang, J., Weschler, C., and Lioy, P.: Ozone and limonene in indoor air: a source of submicron particle exposure, *Environ. Health Persp.*, 108, 1139–1145, 2000. 31085
- Weber, R. J., Sullivan, A. P., Peltier, R. E., Russell, A., Yan, B., Zheng, M., de Gouw, J., Warneke, C., Brock, C., Holloway, J. S., Atlas, E. L., and Edgerton, E.: A study of secondary organic aerosol formation in the anthropogenic-influenced Southeastern United States, *J. Geophys. Res.-Atmos.*, 112, D13302, doi:10.1029/2007JD008408, 2007. 31085
- Wegener, R., Brauers, T., Koppmann, R., Bares, S. R., Roher, F., Tillmann, R., Wahner, A., Hansel, A., and Wisthaler, A.: Simulation chamber investigation of the reactions of ozone with short-chained alkenes, *J. Geophys. Res.*, 112, D13301, doi:10.1029/2006JD007531, 2007. 31086
- Wooldridge, P. J., Perring, A. E., Bertram, T. H., Flocke, F. M., Roberts, J. M., Singh, H. B., Huey, L. G., Thornton, J. A., Wolfe, G. M., Murphy, J. G., Fry, J. L., Rollins, A. W., LaFranchi, B. W., and Cohen, R. C.: Total Peroxy Nitrates (ΣPNs) in the atmosphere: the Thermal Dissociation-Laser Induced Fluorescence (TD-LIF) technique and comparisons to speciated PAN measurements, *Atmos. Meas. Tech.*, 3, 593–607, doi:10.5194/amt-3-593-2010, 2010. 31087

Secondary organic aerosol from NO₃+limonene

J. L. Fry et al.

Title Page

Abstract

Introduction

Conclusions

References

Tables

Figures

◀

▶

◀

▶

Back

Close

Full Screen / Esc

Printer-friendly Version

Interactive Discussion



Table 1. Parameters that were tuned in this model to best fit the observational data, along with the observational constraints used to determine best fit.

Tuned parameter	Observational constraint	Value used in model
Rate of NO ₃ +LIM	Limonene decay; total NO ₃ +N ₂ O ₅ , hours 4–7	6.0×10^{-12} , Calvert et al., 2000 ($\div 2$)
Rate of NO ₃ +O3LIM	Alkyl nitrate formation after 1st injection	0
Ratio of rates of NO ₃ +endo vs. exo C=C	Overall NO ₃ /N ₂ O ₅ shape after 1st injection	30
Rate of NO ₃ +later-gen. aldehydes	HNO ₃ production	50×NO ₃ +HCHO rate
Tuning factors for all ρ_{vap}	Gas/aerosol partitioning of nitrate after 1st injection; organic / nitrate aerosol loading	See Table 3
$\gamma_{\text{NO}_3\text{-aerosol}}$	Gas/aerosol partitioning of nitrate after 2nd injection	0.2

Table 2. Reaction rate constants and branching ratios used in gas-phase portion of kinetics box model. For structures corresponding to variable names, see reaction scheme figure.

Reaction	Branching ratio	Rate constant ($\text{cm}^3 \text{molec}^{-1} \text{s}^{-1}$, 298 K unless otherwise indicated)	Reference/Notes
$\text{NO}_2 + \text{O}_3 \rightarrow \text{NO}_3$		JPL T-dependent rate; 3.2×10^{-17}	JPL Kinetics Eval 15, July 2007
$\text{NO}_3 + \text{NO}_2 \rightarrow \text{N}_2\text{O}_5$		JPL T-dependent rate; 1.0×10^{-12}	JPL Kinetics Eval 15, July 2007
$\text{N}_2\text{O}_5 \rightarrow \text{NO}_3 + \text{NO}_2$		$2.13 \times 10^{-27} \times \exp(11025/T)$	Based on equilibrium constant measured at Juelich, July 2007
$\text{NO}_3 + \text{LIM} \rightarrow \text{ENDONO3}$	0.14	6.0×10^{-12}	Calvert et al., 2000 (+2)
$\text{NO}_3 + \text{LIM} \rightarrow \text{ENDOLIM} + \text{NO}_2$	0.86	6.0×10^{-12}	ibid.
$\text{NO}_3 + \text{LIM} \rightarrow \text{EXONO3}$	0.32	2.0×10^{-13}	Above +30, see text
$\text{NO}_3 + \text{LIM} \rightarrow \text{LIMONE} + \text{HCHO}$	0.68	2.0×10^{-13}	ibid.
$\text{NO}_3 + \text{EXONO3} \rightarrow \text{DINO3}$	0.14	6.0×10^{-12}	Same as rate at endo bond in bare limonene
$\text{NO}_3 + \text{EXONO3} \rightarrow \text{DIKETONO3}$	0.86	6.0×10^{-12}	ibid.
$\text{NO}_3 + \text{LIMONE} \rightarrow \text{KETONO3}$	0.14	6.0×10^{-12}	ibid.
$\text{NO}_3 + \text{LIMONE} \rightarrow \text{TRIKET}$	0.86	6.0×10^{-12}	ibid.
$\text{NO}_3 + \text{ENDONO3} \rightarrow \text{DINO3}$	0.32	2.0×10^{-13}	Same as rate at exo bond in bare limonene
$\text{NO}_3 + \text{ENDONO3} \rightarrow \text{KETONO3} + \text{HCHO} + \text{NO}_2$	0.68	2.0×10^{-13}	ibid.
$\text{NO}_3 + \text{ENDOLIM} \rightarrow \text{DIKETONO3}$	0.32	2.0×10^{-13}	ibid.
$\text{NO}_3 + \text{ENDOLIM} \rightarrow \text{TRIKET}$	0.68	2.0×10^{-13}	ibid.
$\text{NO}_3 + \text{TRIKET} \rightarrow \text{G3KET} + \text{HNO}_3$		2.9×10^{-14}	$50 \times$ rate of $\text{NO}_3 + \text{HCHO}$; see text
$\text{NO}_3 + \text{G2O3} \rightarrow \text{G3O3} + \text{HNO}_3$		2.9×10^{-14}	ibid.
$\text{NO}_3 + \text{DIKETONO3} \rightarrow \text{G3NO3} + \text{HNO}_3$		2.9×10^{-14}	ibid.
$\text{O}_3 + \text{LIM} \rightarrow \text{O3LIM} (\text{endo})$		1.7×10^{-16}	85% of total $\text{O}_3 + \text{LIM}$, Calvert et al., 2000
$\text{O}_3 + \text{LIM} \rightarrow \text{O3LIM2} (\text{exo})$		3.0×10^{-17}	15% of total $\text{O}_3 + \text{LIM}$, Calvert et al., 2000
$\text{O}_3 + \text{O3LIM} \rightarrow \text{G2O3} = \text{TRIKET}$		3.0×10^{-17}	Same as rate at exo bond in bare limonene
$\text{O}_3 + \text{O3LIM2} \rightarrow \text{G2O3} = \text{TRIKET}$		1.7×10^{-16}	Same as rate at endo bond in bare limonene
$\text{NO}_3 + \text{O3LIM} \rightarrow \text{O3LIMNO3}$		$< 4.0 \times 10^{-15}$	Rate of $\text{NO}_3 + \text{LIM} (\text{exo}) + 50$ is upper limit; see text
$\text{NO}_3 + \text{O3LIM2} \rightarrow \text{O3LIM2NO3} = \text{KETONO3}$		$< 1.2 \times 10^{-13}$	Rate of $\text{NO}_3 + \text{LIM} (\text{endo}) + 50$ is upper limit; see text
$\text{O}_3 + \text{ENDONO3} \rightarrow \text{O3LIM2NO3} = \text{KETONO3}$		3.0×10^{-17}	Same as rate at exo bond in bare limonene
$\text{O}_3 + \text{ENDOLIM} \rightarrow \text{G2O3} = \text{TRIKET}$		3.0×10^{-17}	Same as rate at exo bond in bare limonene
$\text{O}_3 + \text{EXONO3} \rightarrow \text{O3LIMNO3} = \text{DIKETONO3}$		1.7×10^{-16}	Same as rate at endo bond in bare limonene
$\text{O}_3 + \text{LIMONE} \rightarrow \text{G2O3} = \text{TRIKET}$		1.7×10^{-16}	Same as rate at endo bond in bare limonene
$\text{NO}_3 + \text{walls} \rightarrow$		6.0×10^{-4}	from NO_3 loss timescale in VOC-free chamber
$\text{N}_2\text{O}_5 + \text{walls} \rightarrow$		7.2×10^{-5}	from N_2O_5 loss timescale in VOC-free chamber
$\text{O}_3 + \text{walls} \rightarrow$		3.9×10^{-6}	from O_3 loss timescale in VOC-free chamber
limonene oxidation products + walls \rightarrow		1.8×10^{-5}	fit to later alkyl nitrate decay

Secondary organic aerosol from NO_3 + limonene

J. L. Fry et al.

Title Page

Abstract

Introduction

Conclusions

References

Tables

Figures



Back

Close

Full Screen / Esc

Printer-friendly Version

Interactive Discussion



Secondary organic aerosol from NO_3 +limonene

J. L. Fry et al.

Table 3. Parameters used in gas-aerosol partitioning portion of the kinetics box model. Calculated vapor pressures were determined using the formalism of Pankow and Asher (2008). For reference, the p_{vap} determined for a pinene monohydroxynitrate was 4.0×10^{-5} Torr (Fry et al., 2009).

Parameter	Calculated value (Torr)	Adjusted value (Torr)	Approx. equivalent structural change
p_{vap} (EXONO3 and ENDONO3)	2.9×10^{-5}	5.8×10^{-7}	Add 2 ketones
p_{vap} (DINO3)	8.2×10^{-10}	8.2×10^{-11}	Add 1 ketone
p_{vap} (KETONO3)	9.6×10^{-6}	9.6×10^{-7}	Add 1 ketone
p_{vap} (DIKETONO3 and O3LIMNO3)	5.0×10^{-7}	5.0×10^{-9}	Add 2 ketones
p_{vap} (TRIKET)	5.8×10^{-3}	5.8×10^{-3}	No change
p_{vap} (O3LIM)	7.4×10^{-5}	7.4×10^{-6}	Add 1 ketone
p_{vap} (G2O3)	3.1×10^{-5}	3.1×10^{-6}	Add 1 ketone

Title Page

Abstract

Introduction

Conclusions

References

Tables

Figures

◀

▶

◀

▶

Back

Close

Full Screen / Esc

Printer-friendly Version

Interactive Discussion



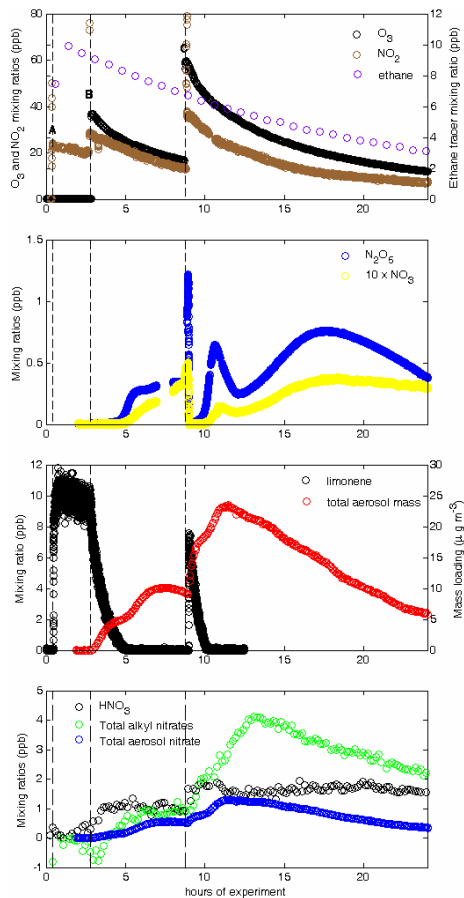


Fig. 1. Overview time series of species monitored. Ethane was used as an inert dilution tracer. Chamber temperature was between 288–296 K for the duration of this experiment.

Secondary organic aerosol from NO₃+limonene

J. L. Fry et al.

Title Page

Abstract

Introduction

Conclusions

References

Tables

Figures

◀

▶

◀

▶

Back

Close

Full Screen / Esc

Printer-friendly Version

Interactive Discussion



Secondary organic aerosol from NO_3 +limonene

J. L. Fry et al.

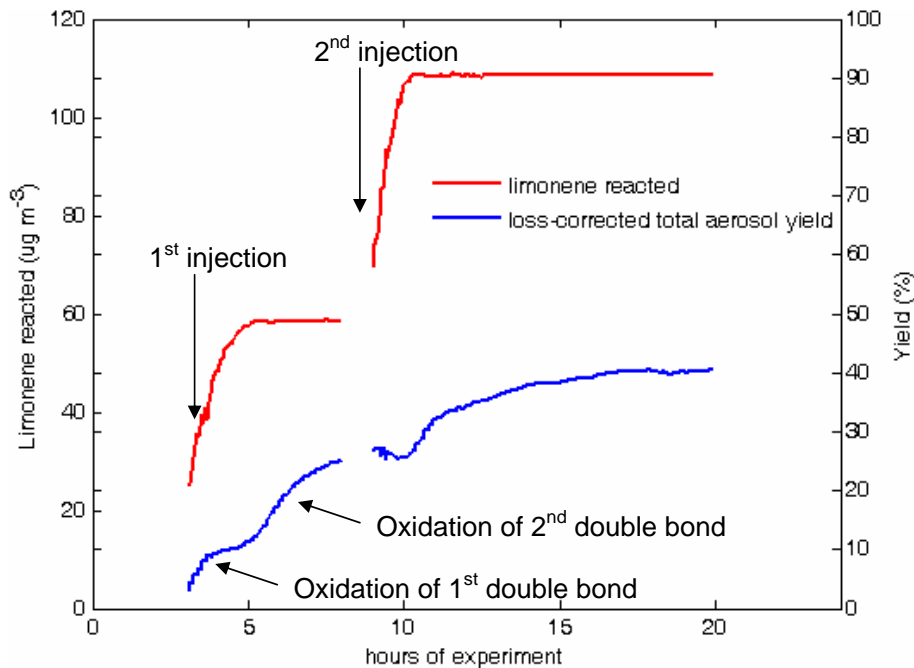


Fig. 2. Total limonene reacted and time-dependent, loss-corrected total aerosol yield for the two limonene injections. Increase in yield after limonene is depleted indicates that reaction at the second double bond in first-generation oxidation products produces aerosol.

Secondary organic aerosol from NO₃+limonene

J. L. Fry et al.

Title Page

Abstract Introduction

Conclusions References

Tables Figures

◀ ▶

◀ ▶

Back Close

Full Screen / Esc

Printer-friendly Version

Interactive Discussion

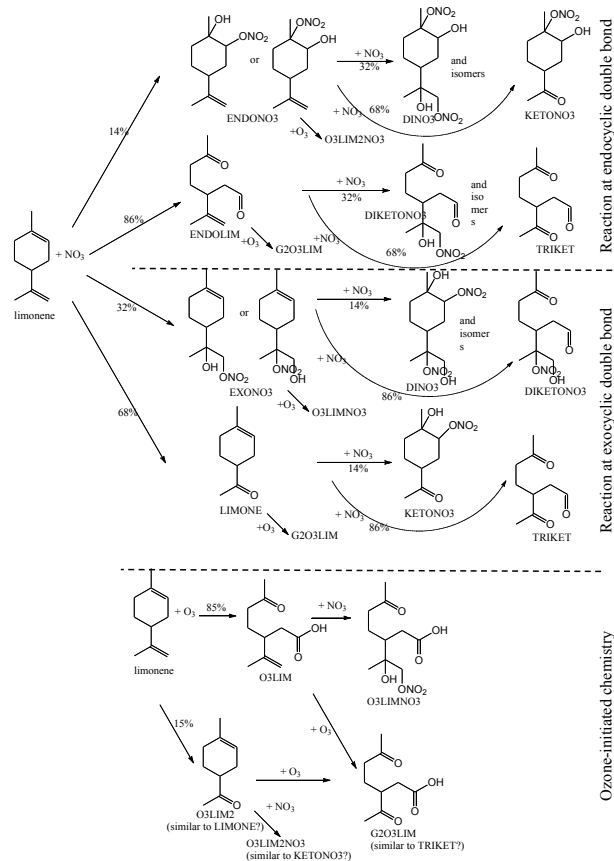


Fig. 3. Reaction scheme of NO₃ and O₃ oxidation of limonene. Structures (especially O₃ products) are proposed approximations; names correspond to individual molecular species tracked in model mechanism.

Secondary organic aerosol from NO_3 +limonene

J. L. Fry et al.

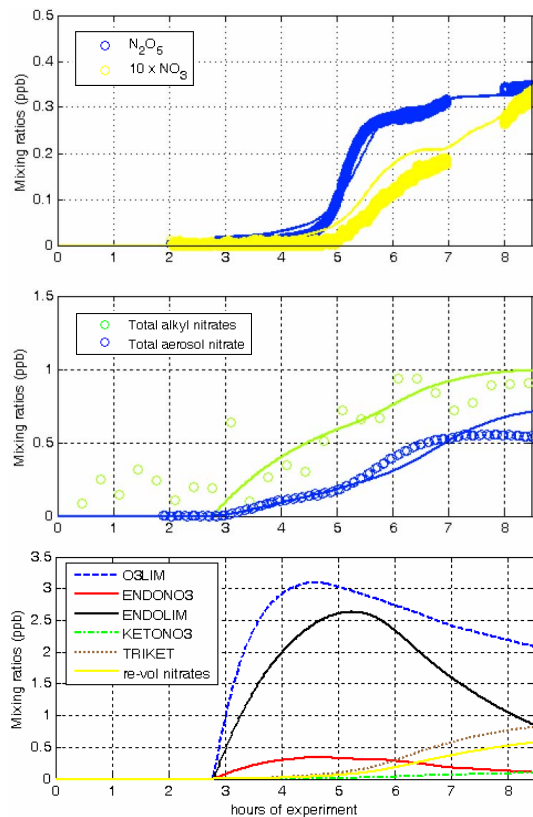


Fig. 4. Measured (markers) and modeled (lines) time traces after the first limonene injection. Bottom panel shows the major products modeled.

[Title Page](#)
[Abstract](#)
[Introduction](#)
[Conclusions](#)
[References](#)
[Tables](#)
[Figures](#)
[◀](#)
[▶](#)
[◀](#)
[▶](#)
[Back](#)
[Close](#)
[Full Screen / Esc](#)
[Printer-friendly Version](#)
[Interactive Discussion](#)


Secondary organic aerosol from NO_3 +limonene

J. L. Fry et al.

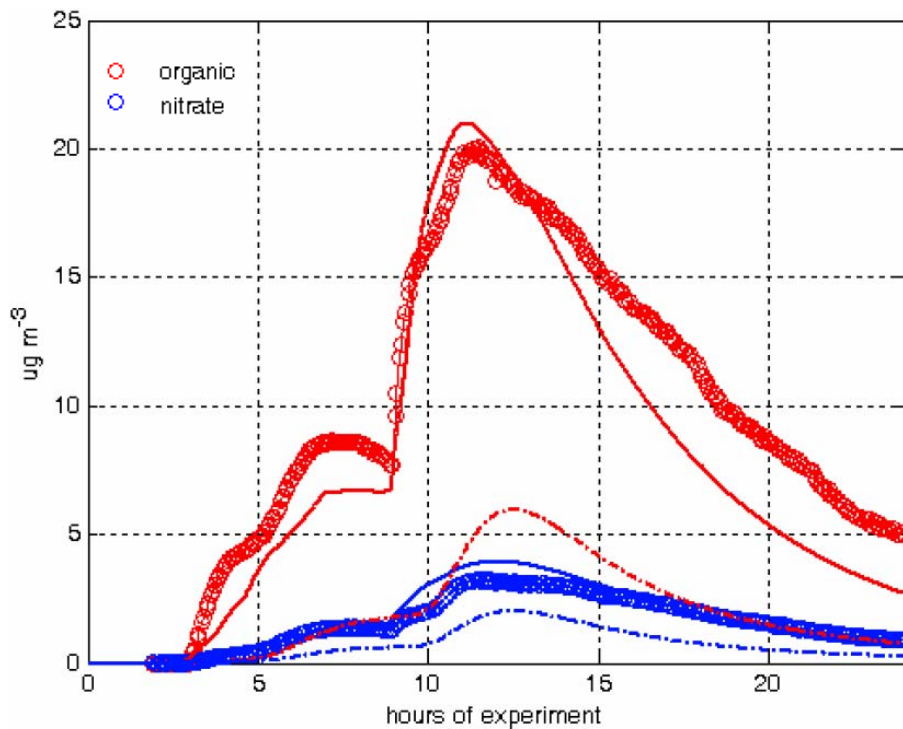


Fig. 5. Change in measurement/model agreement of AMS-measured aerosol organic and aerosol nitrate mass loading before (dashed lines) and after (solid) tuning predicted vapor pressures.

[Title Page](#)[Abstract](#)[Introduction](#)[Conclusions](#)[References](#)[Tables](#)[Figures](#)[◀](#)[▶](#)[◀](#)[▶](#)[Back](#)[Close](#)[Full Screen / Esc](#)[Printer-friendly Version](#)[Interactive Discussion](#)

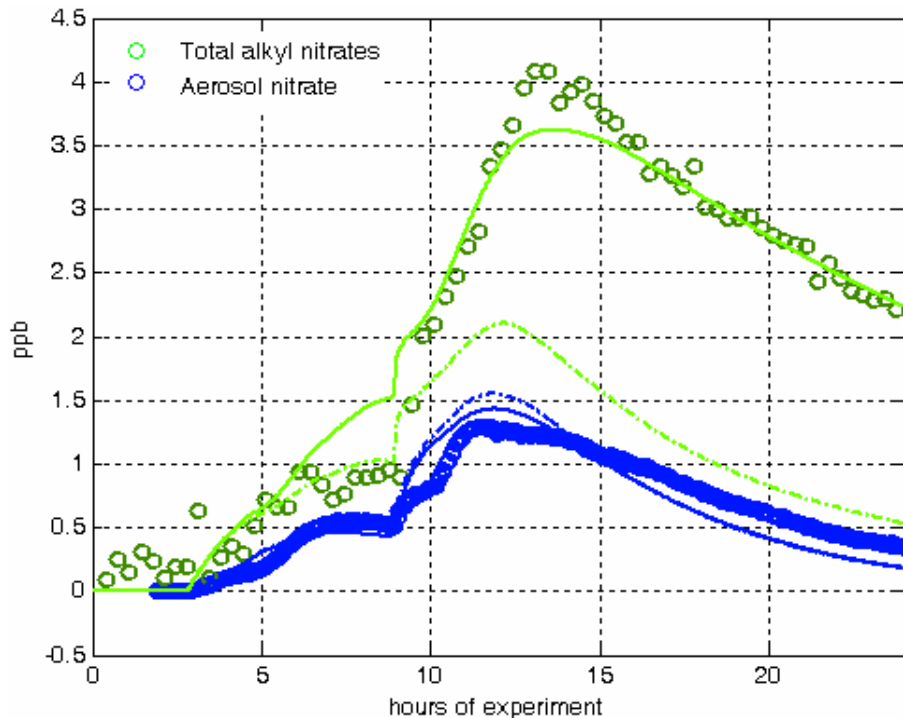


Fig. 6. Change in measurement/model agreement of aerosol and total nitrate without (dashed lines) and with (solid) inclusion in the model of NO_3 uptake and revolatilization of organic nitrate. An uptake coefficient of $\gamma=0.5$ onto the double-bond containing fraction of aerosol gives the best agreement, equivalent to an overall uptake coefficient on this aerosol of $\gamma=0.05\text{--}0.2$. While the addition of this uptake process does not appreciably change the modeled nitrate aerosol, it does drop peak organic aerosol concentrations by about $5\ \mu\text{g m}^{-3}$, from 26 to $21\ \mu\text{g m}^{-3}$. The optimized model traces in Fig. 5 include this uptake process.

**Secondary organic
aerosol from
NO₃+limonene**

J. L. Fry et al.

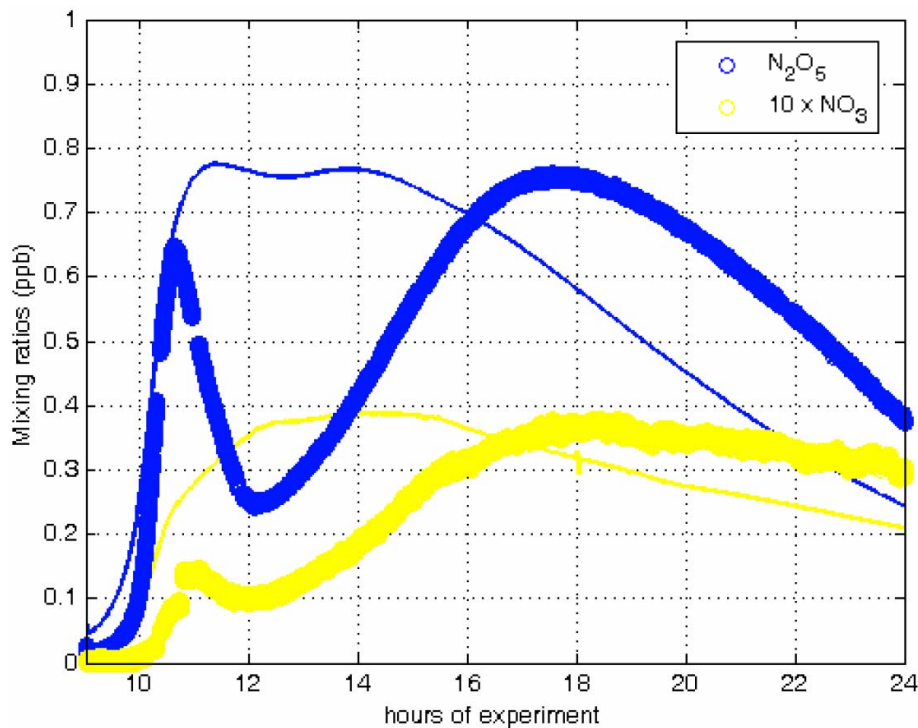


Fig. 7. Measurement/model agreement of NO_3 and N_2O_5 after the second limonene injection. No reasonable permutations of model parameters achieved better agreement with the NO_3 “dip”.

[Title Page](#)[Abstract](#)[Introduction](#)[Conclusions](#)[References](#)[Tables](#)[Figures](#)[◀](#)[▶](#)[◀](#)[▶](#)[Back](#)[Close](#)[Full Screen / Esc](#)[Printer-friendly Version](#)[Interactive Discussion](#)

**Secondary organic
aerosol from
NO₃+limonene**

J. L. Fry et al.

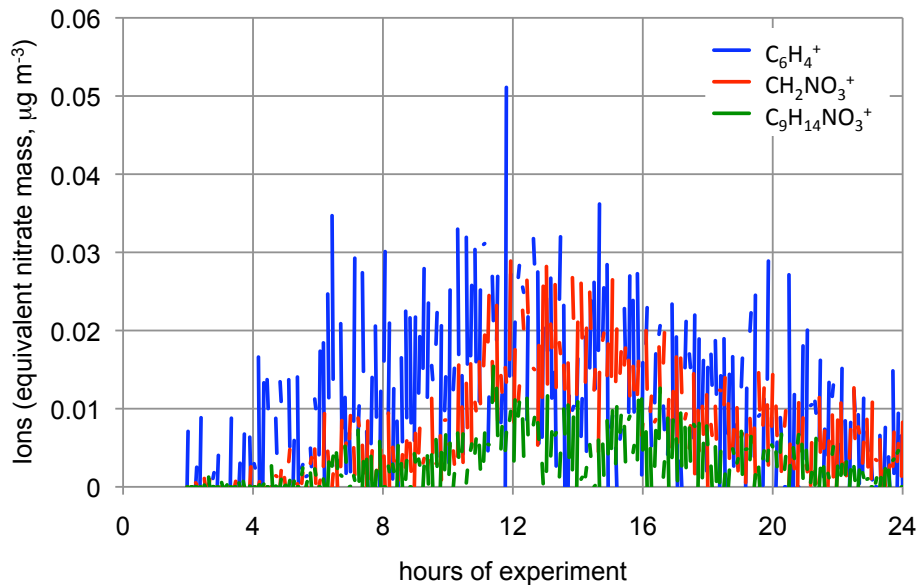


Fig. 8. AMS-detected organo-nitrates fragments. For reference, $C_6H_4^+$ is also shown, a fragment which occurs at the same nominal m/z as $CH_2NO_3^+$.

[Title Page](#)[Abstract](#)[Introduction](#)[Conclusions](#)[References](#)[Tables](#)[Figures](#)[◀](#)[▶](#)[◀](#)[▶](#)[Back](#)[Close](#)[Full Screen / Esc](#)[Printer-friendly Version](#)[Interactive Discussion](#)

Secondary organic
aerosol from
NO₃+limonene

J. L. Fry et al.

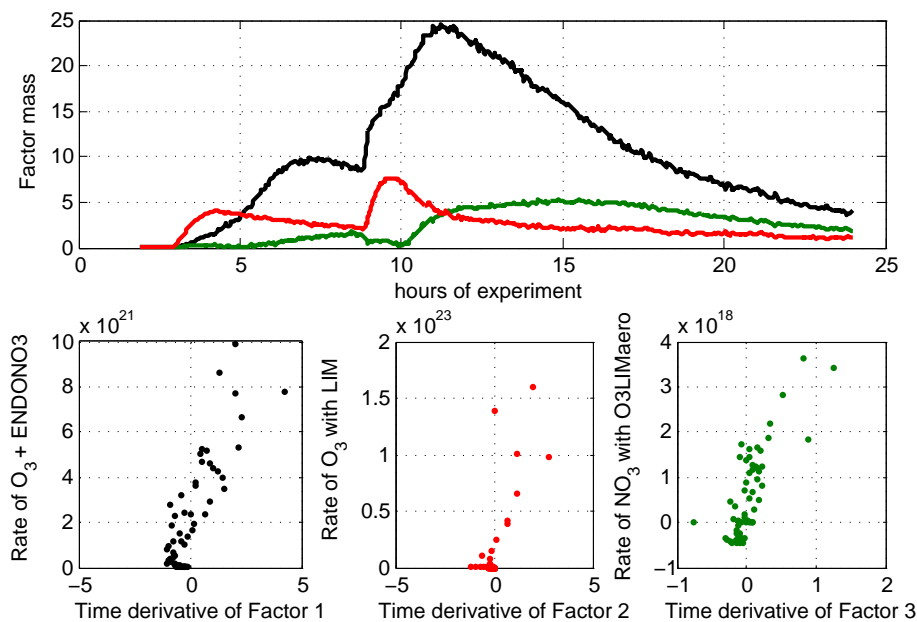


Fig. 9. Summary of PMF results. Upper panel: measured mass in each factor (1: black, 2: red, and 3: green). After these three mass factors, residuals were below $\pm 2\%$ for the entire experiment. Lower panels: correlation plots of the time derivative of each factor with the rate of the best correlated chemical process.

Title Page

Abstract

Introduction

Conclusions

References

Tables

Figures

◀

▶

◀

▶

Back

Close

Full Screen / Esc

Printer-friendly Version

Interactive Discussion



**Secondary organic
aerosol from
NO₃+limonene**

J. L. Fry et al.

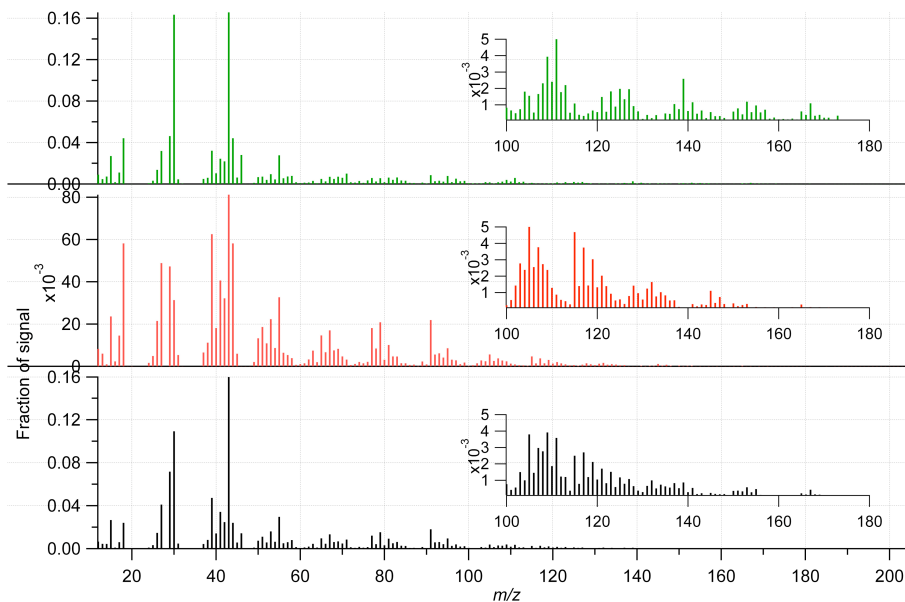


Fig. 10. Mass spectra of the three factors derived from PMF analysis with inserts showing expanded views. Factor one (black) is characterized by a large contribution from m/z 43 and significant 30 and 46. Factor two (red) has a significant signal on m/z 44 and 39, suggesting oxidized organics, and has no contribution from the nitrate masses. Factor three (green) has the largest relative contribution from nitrate masses and larger contributions on $m/z > 100$ than factor 1.

Title Page

Abstract

Introduction

Conclusions

References

Tables

Figures

◀

▶

◀

▶

Back

Close

Full Screen / Esc

Printer-friendly Version

Interactive Discussion

